Development of Improved Algorithms and Multiscale Modeling Capability with SUNTANS

Oliver B. Fringer
473 Via Ortega, Room 187
Dept. of Civil and Environmental Engineering
Stanford University
Stanford, CA 94305
phone: (650) 725-6878 fax: (650) 725-9720 email: fringer@stanford.edu

Award Number: N00014-10-1-0521
http://suntans.stanford.edu

LONG-TERM GOALS

The long-term goal is to develop a nonhydrostatic, parallel ocean simulation tool that is capable of simulating processes on a wide range of scales through use of accurate numerical methods and high-performance computational algorithms. The tool will be applied to study highly nonlinear internal waves in coastal domains to develop an improved understanding of mechanisms that govern their generation, propagation, and dissipation.

OBJECTIVES

The primary objective is to enhance the capabilities of the SUNTANS model through development of algorithms to study multiscale processes in estuaries and the coastal ocean. This involves development of 1) improved momentum and scalar advection on unstructured, staggered grids, 2) accurate and efficient algorithms for solution of the nonhydrostatic pressure, and 3) adaptive grid capabiliites with adaptive mesh refinement and model nesting.

APPROACH

This work focuses on the continued development of SUNTANS (Stanford Unstructured Nonhydrostatic Terrain-following Adaptive Navier-Stokes Simulator), a free-surface, nonhydrostatic, unstructured-grid, parallel coastal ocean and estuary simulation tool that solves the Navier-Stokes equations under the Boussinesq approximation (Fringer et al.,2006). The formulation is based on the method outlined by Casulli and Walters (2000), in which the free-surface and vertical diffusion are discretized with the theta method which eliminates the Courant condition associated with fast free-surface waves and the elevated friction term associated with small vertical grid spacing at the free-surface and bottom boundary. For flows with extensive wetting and drying, advection of momentum is accomplished with the semi-Lagrangian advection scheme (Wang et al. 2011a), which ensures stability in the presence of cells that fill and empty with the tides. Scalar advection is accomplished semi-implicitly and continuity of volume and mass are guaranteed for the hydrostatic solver. The theta

Report Documentation Page

Form Approved
OMB No. 0704-0188

1. REPORT DATE	2. REPORT TYPE	3. DATES COVERED
30 SEP 2013		**00-00-2013 to 00-00-2013**

4. TITLE AND SUBTITLE	5a. CONTRACT NUMBER
Development of Improved Algorithms and Multiscale Modeling Capability with SUNTANS	5b. GRANT NUMBER
	5c. PROGRAM ELEMENT NUMBER
6. AUTHOR(S)	5d. PROJECT NUMBER
	5e. TASK NUMBER
	5f. WORK UNIT NUMBER
7. PERFORMING ORGANIZATION NAME(S) AND ADDRESS(ES) **Stanford University,Dept. of Civil and Environmental Engineering,473 Via Ortega, Room 187,Stanford,CA,94305**	8. PERFORMING ORGANIZATION REPORT NUMBER
9. SPONSORING/MONITORING AGENCY NAME(S) AND ADDRESS(ES)	10. SPONSOR/MONITOR'S ACRONYM(S)
	11. SPONSOR/MONITOR'S REPORT NUMBER(S)

12. DISTRIBUTION/AVAILABILITY STATEMENT
Approved for public release; distribution unlimited

13. SUPPLEMENTARY NOTES

14. ABSTRACT

15. SUBJECT TERMS

16. SECURITY CLASSIFICATION OF:			17. LIMITATION OF ABSTRACT	18. NUMBER OF PAGES	19a. NAME OF RESPONSIBLE PERSON
a. REPORT **unclassified**	b. ABSTRACT **unclassified**	c. THIS PAGE **unclassified**	**Same as Report (SAR)**	**11**	

method for the free surface yields a two-dimensional Poisson equation, and the nonhydrostatic pressure is governed by a three-dimensional Poisson equation. These are both solved with the preconditioned conjugate gradient algorithm with Jacobi and block-Jacobi preconditioning, respectively. Because the nonhydrostatic component of SUNTANS is essentially a correction to the hydrostatic component, SUNTANS can be run seamlessly in nonhydrostatic or hydrostatic modes. SUNTANS is written in the C programming language, and the message-passing interface (MPI) is employed for use in a distributed-memory parallel computing environment. SUNTANS employs the generalized length scale approach to Reynolds-averaged turbulence modeling (Wang et al. 2011b). The SUNTANS grid employs z-levels in the vertical and is unstructured in plan, which enables the resolution of complex coastlines and topographic features. Unstructured grids also enable the use of high grid resolution in regions of interest while coarsening the grid in regions where grid resolution is not required, thereby significantly reducing computational overhead.

WORK COMPLETED

We have completed the development of a nonhydrostatic isopycnal-coordinate model and have performed simulations to study the nonlinear effects of internal wave generation over an idealized Gaussian ridge. We have also performed high-resolution simulations of breaking internal waves on slopes and computed mixing and dissipation. Below results are presented for the isopycnal-coordinate model and the internal wave generation.

RESULTS

Nonhydrostatic isopycnal-coordinate modeling

We have nearly completed a manuscript reporting the formulation and testing of a nonhydrostatic isopycnal coordinate ocean model, which to our knowledge represents the first of its kind. The motivation for this model comes from the success and efficiency of traditional (hydrostatic) isopycnal-coordinate models. Isopycnal coordinates naturally represent a stratified fluid, which in turn reduces the number of grid points from O(100) grid points in traditional ocean models (as in Zhang et al. 2011) to O(1) grid points. This represents a significant reduction in computational effort. Traditional (hydrostatic) isopycnal-coordinate models have been applied to simulating internal waves in the South China Sea (Simmons et al. 2011). However, hydrostatic models don't compute physical dispersion and thus modeled solitary waves are non-physical (they arise from a balance between nonlinearity and spurious numerical dispersion, as discussed in Vitousek and Fringer 2011). We have developed a nonhydrostatic isopycnal-coordinate ocean model to overcome this limitation and to allow the formation of solitary waves with an isopycnal coordinate formulation. Ideally, in locations where the internal wave structure is predominantly mode-1, an isopycnal model with just two layers may suffice.

Our nonhydrostatic isopycnal-coordinate model is intended to be flexible (using an arbitrary number of layers) and straightforward (resembling existing ocean models). We employ a second-order accurate (in space and time) finite-difference/finite-volume formulation on a staggered C-grid as in traditional isopycnal-coordinate models. However, our model uses an implicit free-surface discretization based on the IMEX multistep methods of Durran and Blossey (2012) rather than traditional mode-splitting. We note that implicit free-surface discretizations are more commonly used in nonhydrostatic ocean models. Our model uses the MPDATA algorithm (Smolarkiewicz and Margolin 1998) to handle

wetting and drying of isopycnal layers. The model solves the nonhydrostatic pressure Poisson equation using either the preconditioned conjugate gradient method or the multigrid algorithm with semi-coarsening in the horizontal and line relaxation in the vertical, a strategy that performs well for solving anisotropic elliptic equations (Briggs et al. 2000).

Idealized test cases show that the model is capable of resolving dispersive wave properties and the formation of nonlinear internal solitary waves. Figure 1 shows some of the arbitrary layer configurations that can be used in the model, while Figure 2 shows the dispersive properties of the hydrostatic and nonhydrostatic isopycnal models which are validated against linear theory. These results suggest that nonhydrostatic effects require more layers even if the stratification is uniform in order to resolve depth-variability associated with nonhydrostatic effects. Figure 3 shows the comparison of the formation of nonlinear internal solitary waves in the SUNTANS (z-level model; Fringer et al. 2006) to the nonhydrostatic isopycnal model with 2 and 10 layers. This test case demonstrates that the nonhydrostatic isopycnal model is capable of representing the formation and propagation of solitary waves. Finally, we demonstrate that, although the model represents a discrete set of layers, it is capable of simulating internal wave behavior in continuously stratified systems. Figure 4 shows a nonhydrostatic isopycnal simulation of oscillatory flow in a continuously stratified fluid over a Gaussian sill. This depth perturbation induces the generation of internal wave beams which radiate away from the sill at an angle that agrees well with the linear theory.

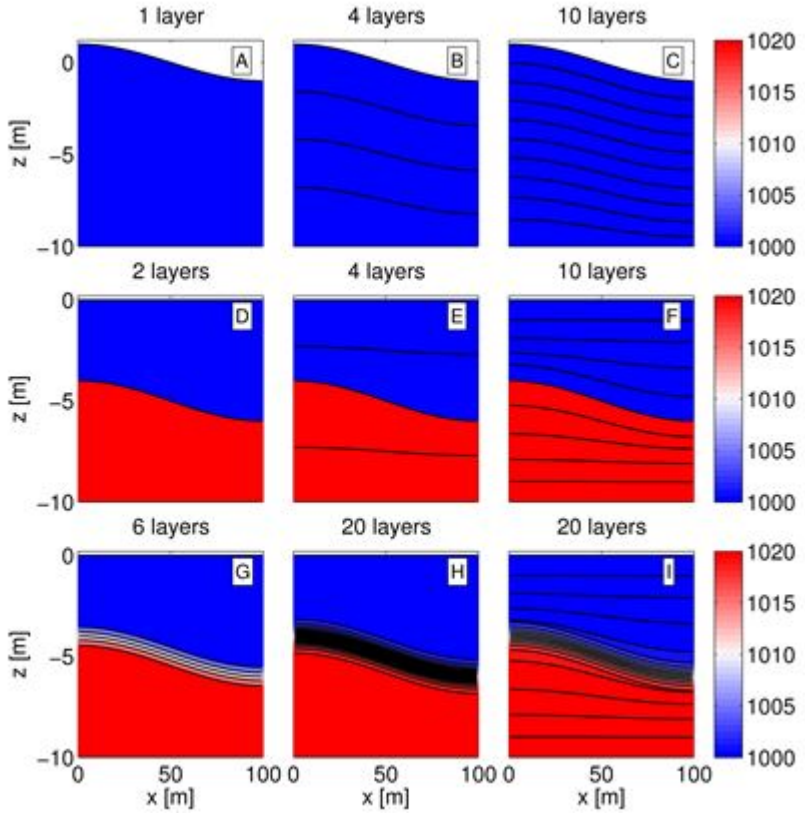

Figure 1: The arbitrary layer configuration used in the nonhydrostatic isopycnal models. Panels A,B and C depict a free surface seiche, panels D,E and F depict a 2-layer internal seiche and panels G,H and I depict an internal seiche with a hyperbolic tangent density profile with varying number of layers.

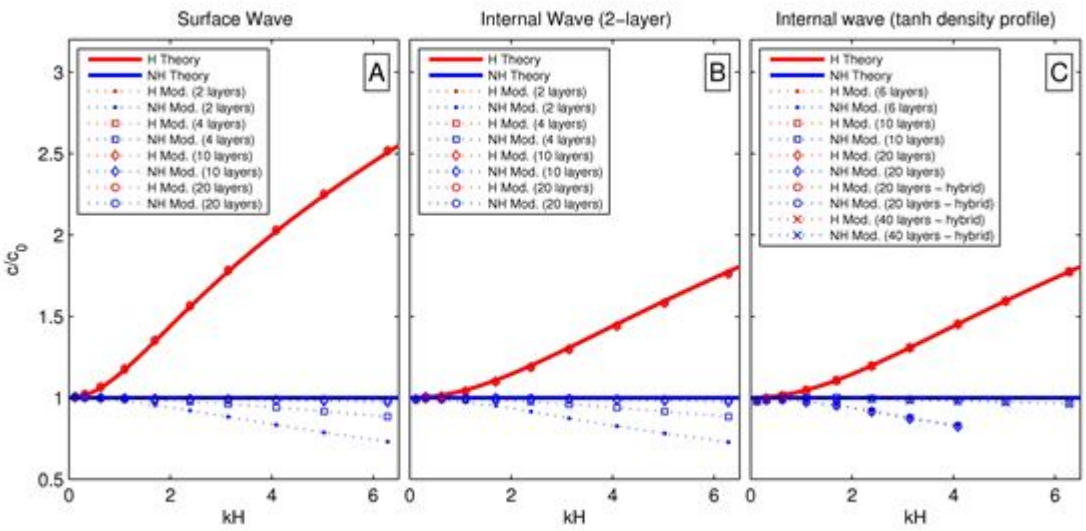

Figure 2: Modeled wave speed normalized by the true wave speed for the hydrostatic (red) and nonhydrostatic (blue) models as a function of aspect ratio (kH) for the free surface, 2-layer and smoothly stratified internal seiche shown in panels A,B and C, respectively. These correspond to columns A, B, and C in Figure 1.

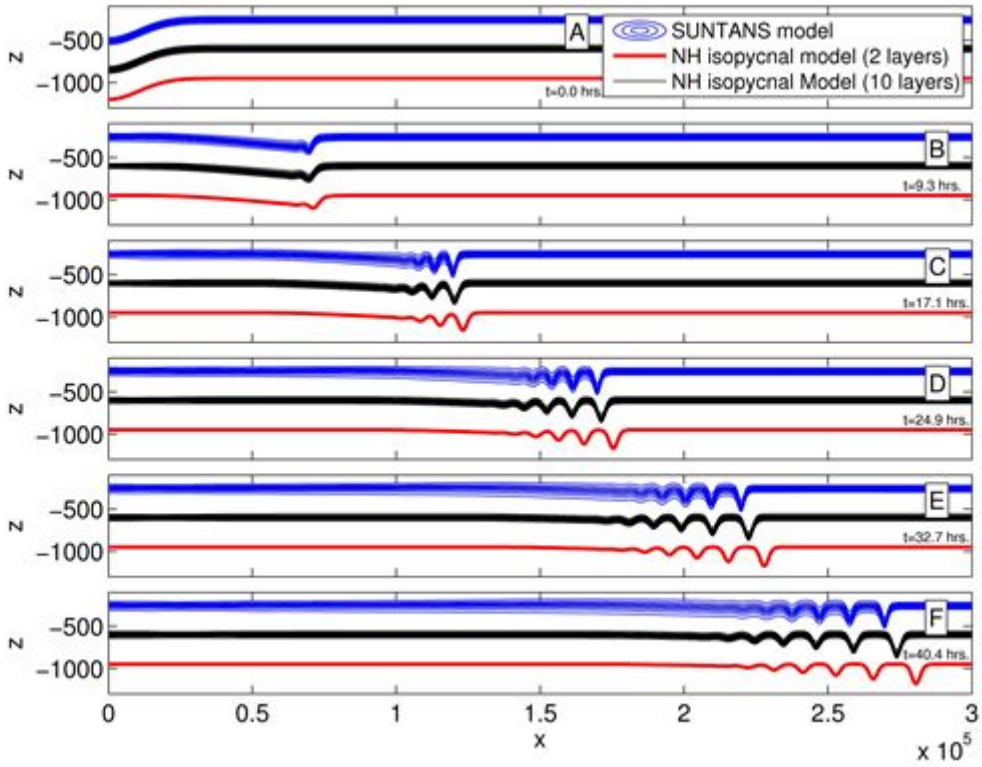

Figure 3: Comparison of the formation of nonlinear internal solitary waves in the SUNTANS z-level model (Fringer et al. 2006) to our nonhydrostatic isopycnal model with 2 and 10 layers. This test case is based on a numerical experiment in Vitousek and Fringer (2011).

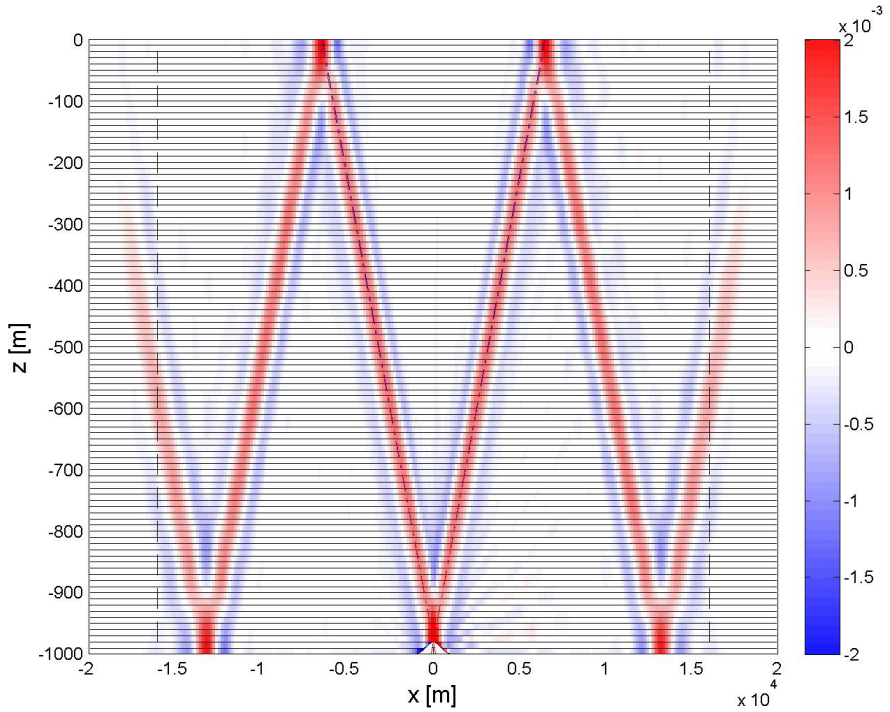

Figure 4: The velocity perturbation (u'=u-U) calculated by the nonhydrostatic isopycnal model as induced by an oscillatory flow in a constantly stratified fluid over a Gaussian sill. Internal wave beams radiate away from the sill at an angle that agrees with linear theory. We note that the magnitude of the velocity perturbation (and the forcing velocity) is kept small so that linear theory is valid.

Nonlinear and nonhydrostatic internal tide generation

The problem of internal tide generation has conventionally been defined by three dimensionless parameters, namely the tidal excursion parameter (ε_2 = tidal excursion/ horizontal topographic scale), the criticality parameter (ε_1 = topographic slope/Internal wave beam slope), and the nondimensional obstacle height (δ = topographic height/total water depth). These parameters are sufficient to describe the problem in the linear limit ($\varepsilon_2 << 1$), and analytical solutions under this approximation require additional limitations of either $\varepsilon_1 << 1$ or $\delta << 1$ or both. Recent advancements in analytical models using Green's functions have eliminated these additional limitations. For example, the iTides model of Echeverri and Peacock (2011) does not require the assumptions of small ε_1 or δ, although a small excursion parameter is still required. Because previous studies have largely been based on linear theory with the aforementioned limitations, nonlinear and nonhydrostatic effects on radiated energy flux are largely unexplored.

We carry out two-dimensional, high-resolution simulations using the SUNTANS model to study nonlinear and nonhydrostatic effects for realistic oceanic flows with ε_2 ~0.03-0.3. The topography consists of an idealized Gaussian ridge centered at *x=0* of the form

$$h(x) = h_0 \exp(-x^2/2\sigma^2),$$

where h_0 is the ridge height and σ is the width of the Gaussian. The domain is forced with a barotropic pressure gradient oscillating at the M_2 tidal frequency ($\omega = 1.41\times10^{-4}$ rad/s). The total water depth is $H = 1000$ m and the initial background buoyancy frequency is uniform at $N = 0.005$ rad/s. We employ a quadrilateral grid (SUNTANS can employ quadrilaterals or triangles or both), and the finest horizontal resolution is employed over the ridge with $\Delta x = 200$ m and linear stretching is employed such that the resolution near the boundaries is ranges from 1400 m to 6000 m (where 6000 m corresponds to the subcritical slope with $\varepsilon_1 = 0.5$ and 1400 m is the highest resolution at the boundaries and corresponds to supercritical slopes with $\varepsilon_1 > 1.75$). A total of 50 grid points is used to discretize the vertical direction and 3800 to 12000 points are employed in the horizontal (the highest number of grid points are used for the case with $\varepsilon_1 = 0.5$), the time step size is $\Delta t = 10$ s, and the total simulation time is 10 tidal periods. We investigate the effect of the criticality parameter varying from subcritical to very supercritical slopes and the nondimensional height parameter on the radiated energy flux for values of the excursion parameter ranging from linear to nonlinear flows. The tidal excursion parameter is defined by $\varepsilon_2 = u_0/(\omega\sigma)$, where u_0 is the barotropic current in deep water away from the ridge, and we vary u_0 but keep ω and σ fixed. The ridge height is chosen to be $h_0 = 750$ *m* which implies a tall ridge with $\delta = 0.75$ and is representative of areas with intense internal tide generation like the Luzon Strait in the South China Sea (e.g. Buijsman et al. 2011) and Kaena ridge at Hawaii (e.g. Carter et al., 2008).

We analyze the variation of the linear baroclinic energy flux (i.e. depth-integrated and time-averaged *p'u'*) as a function of the criticality parameter. In the figures, the theoretical flux is obtained with the iTides model (Echevery and Peacock, 2010), and results from the linearized and hydrostatic SUNTANS model are also computed for comparison. All results are normalized by the theoretical maximum energy flux which is given by the knife-edge result of St. Laurent et al. (2003) that occurs in the limit $\varepsilon_2 \to \infty$ for finite δ. To obtain linear, hydrostatic SUNTANS results, the nonhydrostatic pressure in SUNTANS is eliminated and the nonlinear terms in the momentum equation are ignored. In the density equation, the nonlinear terms are eliminated to yield the linear density equation

$$\frac{\partial \rho}{\partial t} = -\frac{\rho_0 N^2}{g} w,$$

where w is the vertical velocity, ρ_0 is the reference density, and g is the gravitational acceleration.

As shown in Figure 5, the iTides and linear SUNTANS results agree for all values of ε_1 and ε_2, implying that, as expected, both models produce the same results independent of ε_2. However, increasing the excursion parameter (right-to-left tiles in Figure 5) produces marked deviation between the nonlinear and nonhydrostatic SUNTANS result and iTides, particularly in the near-critical range $\varepsilon_1 = 0.75$-1.75. Figure 6 shows the ratio of the energy flux computed by the nonlinear and nonhydrostatic SUNTANS model to the linear result computed by iTides, and indicates that there is a minimum in the radiated energy flux when the slope is near-critical. When the slope is exactly critical, nonlinear effects induce a drop of 85% in the radiated energy flux.

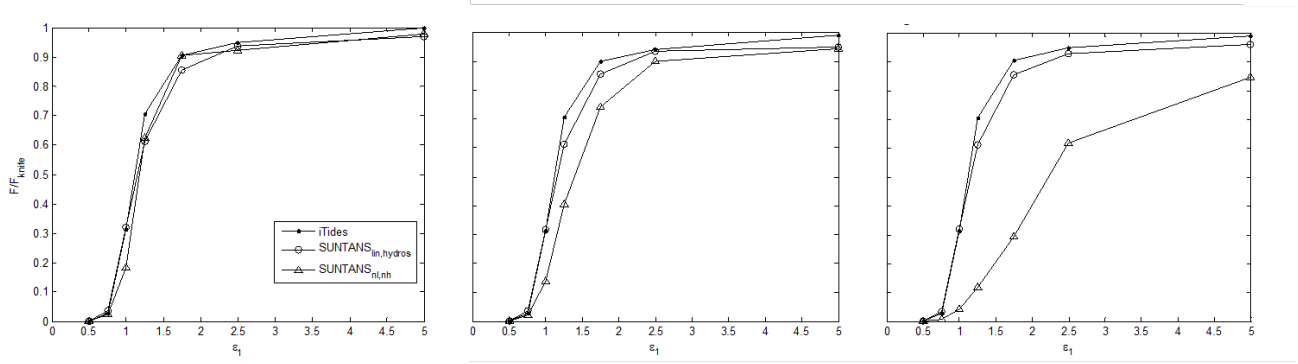

Figure 5: Comparison of three different models and how they compute the effect of the criticality parameter ε_1 on the baroclinic energy flux radiating from a Gaussian ridge for three different excursion parameters (left: ε_2=0.03, middle: ε_2=0.1; right: ε_2=0.3) when δ=0.75. The energy flux is nondimensionalized by the knife-edge energy flux from St. Laurent et al. (2003).

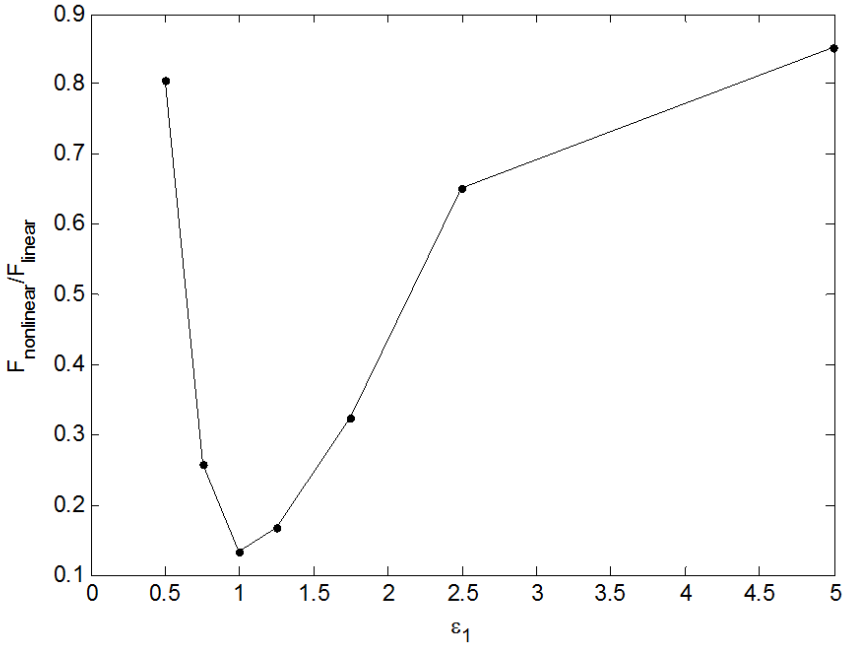

Figure 6: Ratio of nonlinear energy flux radiating from a Gaussian ridge to the linear energy flux computed by iTides as a function of the criticality parameter ε_1 when ε_2=0.3 and δ=0.75.

Figure 7 shows that the drop in energy flux for large excursion parameters and near-critical slopes depends to great extent on the height of the ridge. Both the nonlinear and nonhydrostatic SUNTANS model and the iTides model predict a drop in the energy flux with increasing ridge height (with ε_1 and ε_2 fixed). Because the iTides model employs a nonlinear kinematic boundary condition at the bottom boundary, it is valid for flows with arbitrary ε_1 and δ, as long as $\varepsilon_2 << 1$. Therefore, the drop in energy flux for large ridge heights predicted by the iTides model is related to nonlinear and inviscid topographic boundary effects and not nonlinear effects within the flow itself or viscous boundary effects such as those that give rise to the nonlinear energy flux terms (e.g. Kang and Fringer 2012) or to breaking and dissipation. These flow-induced nonlinear effects give rise to further losses in the

energy flux as indicated by the lower energy flux computed by the SUNTANS model as compared to iTides.

The relative effects of nonlinearity within the flow to those computed by iTides can be understood from Figure 8, which shows a plot of the ratio of the SUNTANS-computed energy flux to that computed by iTides. As the ridge height increases, the relative impact of nonlinearity within the flow on the energy flux increases. When $\delta=0.75$, the flux computed by SUNTANS is only 25% of that computed by iTides. Because the iTides model produces a decreased energy flux for large δ, it is clear that much of the reduction in energy flux with increased δ is not a result of an increase in the nonlinear energy flux terms of Kang and Fringer (2012). We hypothesize that the reduction is due to redirection of barotropic energy to generation of boundary currents for taller ridges which results in a lower conversion of barotropic-to-baroclinic energy flux. Following the work of Winters and Armi (2013), we are studying the problem in terms of newly defined inner flow variables which more accurately represent the strongly nonlinear flow over the ridge, rather than the outer flow variables ε_1, ε_2, and δ that were used in this study as well as throughout the literature on internal wave generation.

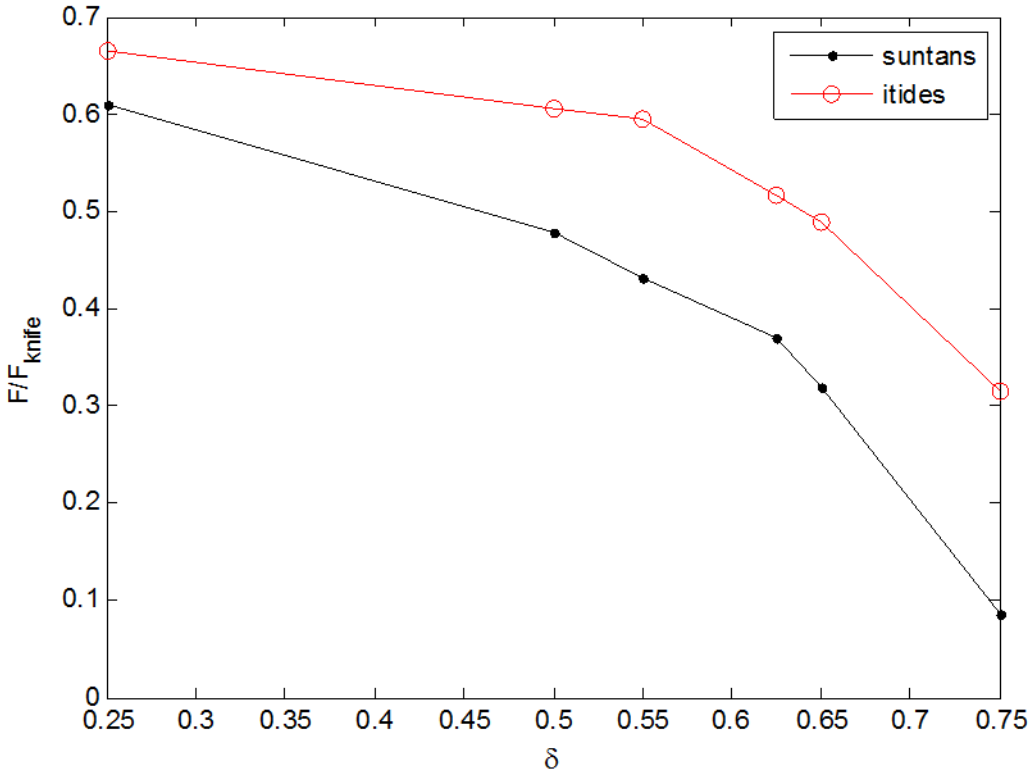

Figure 7: Effect of the nondimensional ridge height δ on the energy flux radiated from a Gaussian Ridge with $\varepsilon_1=1$ and $\varepsilon_2=0.3$ as computed by the linear iTides model and the SUNTANS model. The energy flux is normalized by the maximum knife-edge value from St. Laurent et al. (2003).

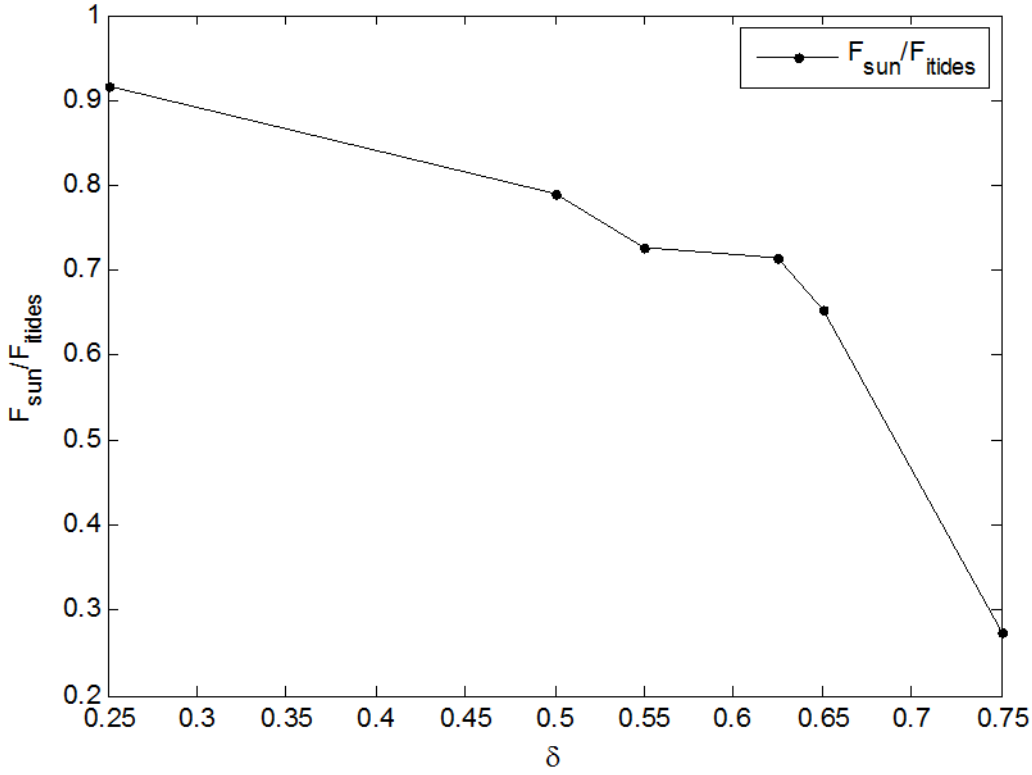

Figure 8: Effect of the nondimensional ridge height δ on the ratio of the energy flux radiated from a Gaussian Ridge as computed by SUNTANS to that computed by the iTides model with ε_1=1 and ε_2=0.3.

IMPACT/APPLICATIONS

High-resolution simulations using nonhydrostatic models like SUNTANS are crucial for understanding multiscale processes that are unresolved, and hence parameterized, in larger-scale ocean models.

REFERENCES

Briggs, William L., V. Emden Henson, and S. F. McCormick, 2000, "A multigrid tutorial", SIAM, Philadelphia, PA (2000).

Buijsman, M. C., Kanarska, Y., & McWilliams, J. C., 2010, "On the generation and evolution of nonlinear internal waves in the South China Sea", Journal of Geophysical Research: Oceans, 115 (C2).

Carter, G. S., Merrifield, M. A., Becker, J. M., Katsumata, K., Gregg, M. C., Luther, D. S., and Firing, Y. L., 2008, "Energetics of M2 barotropic-to-baroclinic tidal conversion at the Hawaiian Islands", Journal of Physical Oceanography, 38(10), 2205-2223.

Casulli, V. and R.A. Walters, 2000, "An unstructured, three-dimensional model based on the shallow water equations", International Journal for Numerical Methods in Fluids, 32, 331-348.

Durran, Dale R., and Peter N. Blossey, 2012, "Implicit-Explicit Multistep Methods for Fast-Wave-Slow-Wave Problems." Monthly Weather Review 140 (4), 1307-1325.

Echeverri, P., & Peacock, T., 2010, “Internal tide generation by arbitrary two-dimensional topography”, Journal of Fluid Mechanics, 659, 247-266.

Fringer, O. B., M. Gerritsen, and R. L. Street, 2006, "An unstructured-grid, finite-volume, nonhydrostatic, parallel coastal ocean simulator." Ocean Modelling 14.3 (2006): 139-173.

Kang, D., and O. B. Fringer, 2012, “Energetics of barotropic and baroclinic tides in the Monterey Bay area”, J. Phys. Oceanogr., 42 (2), 272-290.

Simmons, H., Chang, M. H., Chang, Y. T., Chao, S. Y., Fringer, O., Jackson, C. R., and Ko, D. S., 2011, “Modeling and prediction of internal waves in the South China Sea”. Oceanography-Oceanography Society, 24(4), 88.

Smolarkiewicz, P. K., & Margolin, L. G., 1998, “MPDATA: a finite-difference solver for geophysical flows”. Journal of Computational Physics, 140(2), 459-480.

St Laurent, L., Stringer, S., Garrett, C., & Perrault-Joncas, D., 2003, “The generation of internal tides at abrupt topography”, Deep Sea Research Part I: Oceanographic Research Papers, 50(8), 987-1003.

Tahvildari, N., Fringer ,O. B., Peacock, T., 2013, “Nonhydrostatic and nonlinear energetics of internal tides over a submerged ridge”, Ocean Turbulence Conference Abstract, CNLS, LANL, Santa Fe, NM, June 2013.

Vitousek, S., and Fringer, O.B., 2011, “Physical vs. numerical dispersion in nonhydrostatic ocean modeling.” Ocean Modelling 40 (1), 72-86.

Wang, B., Zhao, G., and Fringer, O. B., 2011a, "Reconstruction of vector fields for semi-Lagrangian advection on unstructured, staggered grids", Ocean Modelling, 40 (1), 52-71.

Wang, B., Giddings, S. N., Fringer, O. B., Gross, E.S., Fong, D. A., and Monismith, S. G., 2011b, "Modeling and understanding turbulent mixing in a macrotidal salt wedge estuary", J. Geophys. Res., 116, C02036.

Winters, K. B., and Armi L. (2013), “The response of a continuously stratified fluid to an oscillating flow past an obstacle”, Journal of Fluid Mechanics. 727, 83-118.

Zhang, Z., Fringer, O. B., and Ramp, S. R., 2011, “Three-dimensional, nonhydrostatic numerical simulation of nonlinear internal wave generation and propagation in the South China Sea”, J. Geophys. Res., 116, C05022.

PUBLICATIONS

Arthur, R. S., Walter, R. K., Woodson, C. B., Fringer, O. B., and S. G. Monismith, 2012, “Field and Numerical Investigation of Nearshore Internal Bores”, 59th Annual Eastern Pacific Ocean Conference (EPOC), September 22, 2012. Mt. Hood, OR.

Fringer, O. B., 2013, “Towards large-eddy simulation of internal waves in the coastal ocean”, Gordon Research Conference on Coastal Ocean Circulation, Biddeford, Maine (invited).

Fringer, O. B., and P. J. Wolfram, 2013, "Dealing with divergence errors and noise in C-grid finite-volume hydrodynamic models", Advances on Computational Mechanics: A Conference Celebrating the 70th Birthday of Thomas J. R. Hughes, San Diego (invited).

Fringer, O. B., Vitousek, S., and P. J. Wolfram, 2012, “Finite-volume, nonhydrostatic ocean modeling on unstructured grids”, 1st International Conference on Frontiers in Computational Physics: Modeling the Earth System, Boulder (invited).

Sankaranarayanan, S., and Fringer, O. B., 2013, "Dynamics of barotropic low-frequency fluctuations in San Francisco Bay during upwelling", Cont. Shelf. Res., 65, 81-96, [published, refereed].

Holleman, R., Fringer, O. B., and Stacey, M. T., 2013, "Numerical diffusion for flow-aligned unstructured grids with application to estuarine modeling", Int. J. Numer. Methods Fluids., 72, 1117-1145, [published, refereed].

Wolfram, P., and O. Fringer, 2012, “Mitigating divergence-error oscillations in triangular C grids for nonlinear and nonhydrostatic flows”, Workshop on Multiscale Modelling of Coastal, Shelf and Ocean Dynamics (IMUM), Delft, Netherlands.

Wolfram, P. J., and Fringer, O. B., 2013, "Mitigating horizontal divergence 'checker-board' oscillations on unstructured triangular C-grids for nonlinear hydrostatic and nonhydrostatic flows", Ocean Modelling, 69, 64-78, [published, refereed].